

Evaluation of soil-geogrid interaction using transparent soil with laser aided imaging

Xin Peng & Jorge G. Zornberg
The University of Texas at Austin, USA

ABSTRACT: The use of geogrids in the design of reinforced soil retaining structures and of stabilized roadways require proper evaluation of the mobilization of the soil-geogrid interaction. In this study, a new experimental system involving the use of transparent soil with laser aided imaging was developed to visualize and quantify the interaction between soil and geogrids. Focus is placed not only on obtaining the displacement field for the geogrid itself but also on defining the displacement field for the surrounding soil particles, at different locations in relation to the soil-geogrid interface. Laser beam with a wavelength of 638 nm and with up to 350 mW output power was adopted to track the solid particles of transparent soil at a plane perpendicular to the soil-geogrid interface. The collimated beam resulted in clear definition of the individual particles at the selected plane within the model. High-definition digital cameras were used to collect images suitable to track the displacement fields of both the geogrid specimen and the solid particles within the laser-illuminated plane. Digital Image Correlation (DIC) techniques were used to define the displacement field based on the captured images. In this paper, results obtained from a prototype test conducted by using a geogrid with rectangular aperture shape are illustrated. The test results allowed evaluation of the geogrid displacement profiles, soil displacement profiles along the loading direction, and shear band development in soil. The experimental system developed in this study, as well as the adopted deformation measurement techniques were found to provide insight on the load transfer mechanisms between soil and geogrids.

Keywords: soil-geogrid interaction, transparent soil, Digital Image Correlation, Laser, shear band

1 INTRODUCTION

Geogrid, one of the most commonly used geosynthetics, is defined as a geosynthetic formed by a regular network of integrally connected elements with apertures greater than 6.35 mm to allow interlocking with surrounding soil, rock, earth, and other surrounding materials to function primarily as reinforcement (ASTM D4439-15a). In applications involving soil retaining structures and roadway systems, geogrids with different features have been extensively used in North America since 1982 (Koerner, 2012). Geogrids have been found to provide (1) good quality control in their manufacture process, (2) fast and easy installation, (3) economic advantages in comparison to the use of traditional construction materials, and (4) good performance in a variety of civil engineering applications. Due to the significant benefits achieved with applications involving geogrids, the market has responded by continuously developing products with different characteristics and using different materials. However, the evaluation of the differences in the performance of many available geogrids has been challenged by the diversity of products, which may render different performances in field applications.

In the case of the geogrid-reinforced soil retaining structures, traditional design methods have been typically based on the limit-equilibrium analyses. On the other hand, geogrid-stiffened roadway systems have been designed using empirical methods, although new promising evaluations are being developed involving the use of deformability properties such as the stiffness of the soil-geosynthetic composite (Zornberg and Roodi 2017, Roodi and Zornberg 2017). However, the actual soil-geogrid interaction be-

havior under service condition is still not fully understood, especially for recognizing the resistance contributions from the different rib components, including the effect of their different geometric characteristics. A comprehensive understanding of the load transfer mechanisms between soil and geogrid under service conditions can provide valuable insight into the determination of the design parameters (e.g. confined stiffness of geogrids, pullout resistance of geogrids, and resilient modulus of the geogrid-involved foundation layers, etc.) of the structures involving the use of geogrids. A number of experimental and numerical studies have been conducted to assess these mechanisms over the past decades (Wilson-Fahmy and Koerner 1993, Ochiai et al. 1996, Ziegler and Timmers 2004, Teixeira et al. 2007). However, previous investigations tended to concentrate on the analyses of the geogrid specimens and neglected the overall soil deformation induced by the movements of geogrids.

The use of transparent soil and laser technology has recently shown significant promise to investigate the performance of geotechnical structures (Iskander 2010, Ezzein and Bathurst 2011, Wallace and Ruthersford 2015, Chini et al. 2015, Ferreira and Zornberg 2015). In this paper, an experimental testing system is introduced to evaluate the overall confined performance of a widely-used geogrid with rectangular aperture shape. Specifically, displacement fields for both the geogrid specimen and the granular media during the pullout test were visualized and measured using transparent soil in conjunction with laser technology and advanced digital image analysis.

2 MATERIALS

2.1 Transparent soil

The solid material employed in this study was crushed fused quartz, which has been previously used by Ferreira (2013). It possesses a median size, D_{50} , of 3.9 mm, an effective size, D_{10} , of 2.5 mm, a uniformity coefficient, C_u , of 1.6, and a coefficient of curvature, C_c , of 1.2. According to the Unified Soil Classification System (USCS), this granular material classifies as a poorly graded sand (SP). The specific gravity of this material at 20°C is 2.203. According to the results of the direct shear tests, the friction angle of the crushed fused quartz is about 44°~45°. In addition, the refractive index (RI) of the crushed fused quartz is 1.4585.

The pore fluid used with the fused particles is a mixture of two clear mineral oils: Puretol 7 and Paraflex HT4. Selected properties of these two liquids are presented in Table 1. As indicated in this table, Puretol 7 has a higher RI than the solid fused quartz, while Paraflex HT4 has a lower RI. Therefore, for the given volume ratio of these two liquids, which is Puretol 7/Paraflex HT4 \approx 52/48, the final combination aimed at having the same refractive index as that of fused quartz.

Table 1. Selected properties of the two components of the liquid mixture (from manufacture's specification sheet^{*}).

Properties	Puretol 7	Paraflex HT4
Density, 15 °C, g/cm ³	0.859	0.836
Viscosity, 40 °C, cSt	12.2	3.8
Color	Clear and bright	Clear and bright
Odor	No odor/slight petroleum oil like	Mild petroleum oil like
Flash point, °C	> 170	> 125
Pour point, °C	-20	-57
Refractive index, 22 °C	1.4635	1.4532
Solubility	Insoluble in water	Insoluble in water
Chemical stability	Stable	Stable
Emergency overview	No specific hazard	No specific hazard

^{*}The two mineral oils are manufactured by Petro-Canada Lubricants Incorporation; Puretol 7 is distributed by Coast Southwest Incorporation, and Paraflex HT4 is distributed by Schmidt and Sons Incorporation.

2.2 Geogrid reinforcement

A geogrid with rectangular aperture shape was used in this study. It was manufactured by punching out holes in polypropylene sheets, and then heating and stretching them along two orthogonal directions. Selected properties of this geogrid product are presented in Table 2.

Table 2. Nominal properties of the geogrid used in this study (from manufacturer’s specification sheet).

Specimen Orientation	Tensile strength @ 5% strain (kN/m)	Aperture shape	Rib	Rib pitch (mm)	Mid-rib depth (mm)	Mid-rib width (mm)
Machine Direction	8.5	Rectangular	Longitudinal	25	0.76*	3.0*
			Transverse	33	0.93*	

* Since the manufacturer does not provide these dimensions, they were determined in this study for the tested specimens.

3 EXPERIMENTAL SETUP AND METHODOLOGY

3.1 Experimental setup

Figure 1 illustrates the frontal view of the experimental apparatus developed for this study. The unconfined portion of the geogrid specimen was attached to the load grip using a clamping system. The load grip was connected to a load cell which was used to measure the frontal pullout load during testing. The other end of the load cell was fixed on the moving head of the load frame, with the speed of the load frame being controlled by a load control system.

A digital camera with a maximum resolution of 24 megapixels (Digital Camera I in Figure 1) was used to track deformations in the confined geogrids, as observed in frontal view of the transparent soil model. Another digital camera with a maximum resolution of 5 megapixels (Digital Camera II in Figure 1) was used to track the displacement field of soil particles in a laser-illuminated plane from the side view of the transparent soil model.

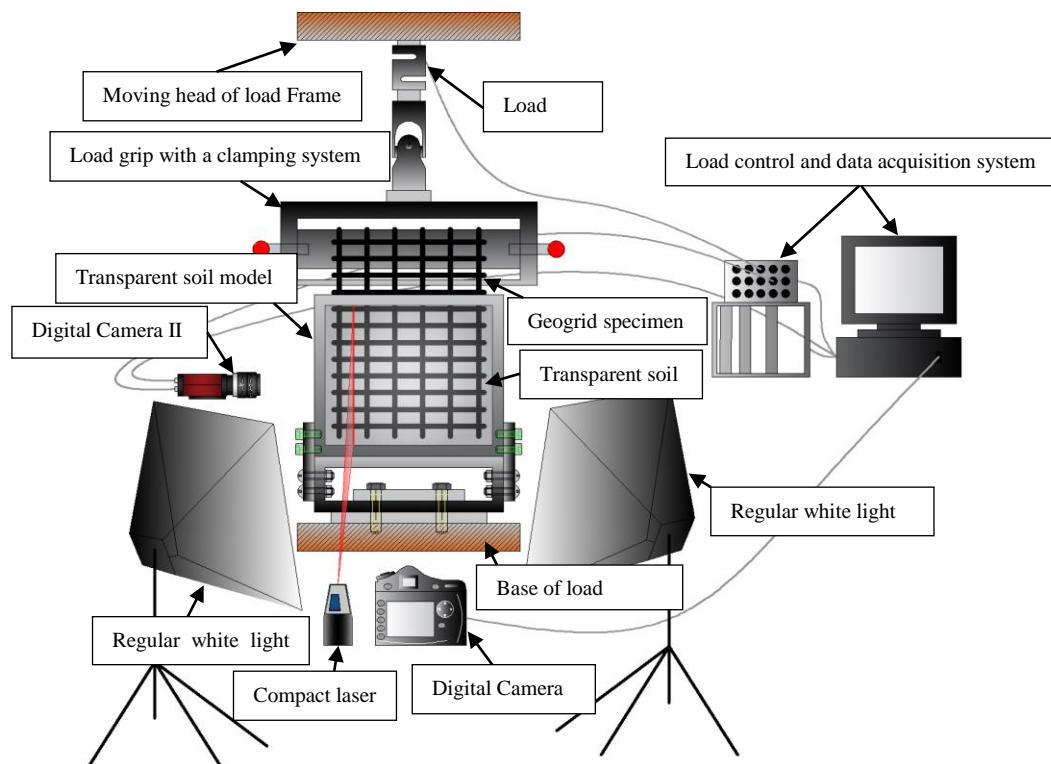


Figure 1. Schematic diagram of the frontal view of the experimental system developed for this study.

To illuminate geogrid specimen, a light system was used to provide comparatively uniform and consistent regular white light to illuminate the transparent soil model. This system was composed of two 160

W photo studio soft boxes. The dimensions of each of the soft boxes were 610 mm long by 406 mm wide, which was large enough to provide comparatively uniform light on the frontal wall of transparent soil model (300 mm long by 250 mm wide). The color temperature of the light bulbs was 6,500 K which is similar to the color of common daylight.

A laser-light sheet with a wavelength of 638 nm (in red color) was shoot from a compact laser system located at the front of the transparent soil model. With the illumination of the laser light, the boundaries of individual fused quartz particles can be visualized within the laser-illuminated plane inside of the transparent soil model. The laser penetration plane was along the perpendicular direction of the soil-geogrid interface as shown in Figure 1.

Because the diffusion of the laser light could contaminate the lighting condition for geogrid tracking using Digital Camera I, a 10-second ON-OFF time combination was adopted for laser shooting. Since the white light source includes light beams with different wavelengths/colors which are neither coherent nor collimated, these light beams could attenuate the contrast of the boundaries of fused quartz particles illuminated by the monochromatic, coherent, and collimated red laser light. Consequently, a red filter was attached to the lens of Digital Camera II to filtrate light beams with colors other than red.

The nominal dimensions of the confined portion of the geogrid specimens were 230 mm long by 200 mm wide. The applied normal stress was 27.6 kN/m², and the loading displacement rate was 1 mm/min.

3.2 Image processing techniques

The displacement tracking method used in the analyses presented in this paper involved Digital Image Correlation (DIC). The DIC code used in this study is an open source MATLAB code developed by Jones (2015). The resolution of this DIC code is 0.1 pixel, since nine discrete cross-correlation coefficients surrounding the absolute maximum coefficient were interpolated using a second order polynomial in both horizontal and vertical directions.

Frontal-view images were used to analyze the confined displacement field of the geogrid specimen via DIC method. Evaluation of the DIC results involving the confined displacement field of the geogrid specimen were previously discussed by Peng and Zornberg (2017). The side-view images were used to analyze the displacement field of the soil particles in the laser-illuminated plane. In the prototype test, the captured side-view image and the calculated soil displacement field at pullout failure are presented in Figure 2. On the left-hand side in Figure 2(a), rib shadows can be observed because the transverse ribs blocked laser light penetration. The shadows moved upward with the movement of the transverse ribs. The moving shadows adversely affected the quality of the DIC analysis for tracking the displacement field of fused quartz particles. Consequently, only the area in front of the geogrid specimen (on the right-hand side in Figure 2(a)) was used for soil displacement tracking.

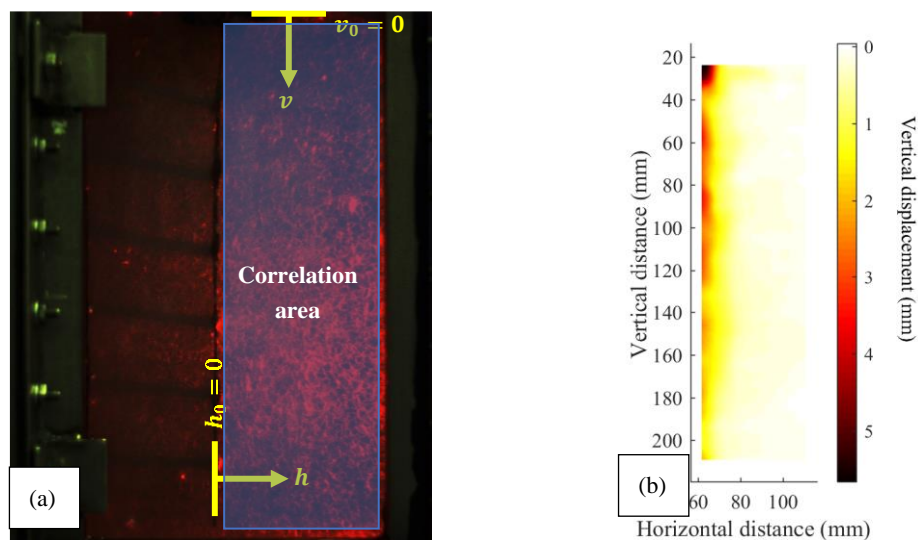


Figure 2. Use of DIC to generate the displacement field of fused quartz particles in a laser-illuminated plane: (a) correlation area in the side-view image, and (b) Displacement field (in the loading direction) of soil particles at the time of pullout failure.

4 TEST RESULTS

In each of the tests, the load data recorded from the load cell was normalized by the actual width of each geogrid specimen to define the unit tension. The relationship between the frontal load (or frontal unit tension) and relative time (or grip displacement) in the prototype test is presented in Figure 3. The grey circles in the plot correspond to the load data measured from the load cell. The orange curve represents the smoothed load data obtained by applying moving average methods. A total of sixteen images (with each image captured at the time indicated with a blue star in Figure 3) were selected for image processing. The average time span between two successive images was about 120 seconds. The last selected image corresponds to the time of pullout failure.

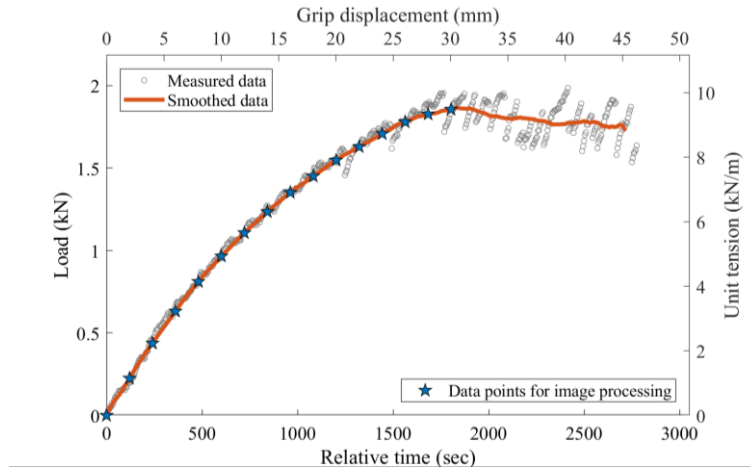


Figure 3. Relationship between the frontal load (or the unit tension) and the relative time (or the grip displacement) in the prototype test.

Details of the geogrid specimen used in the test and the selected test results are summarized in Table 3.

Table 3. Details of the testing specimen used in the prototype test and the selected test results.

Specimen width (mm)	Number of Longitudinal ribs	Mass per unit area (g/m ²)	Ultimate pullout load (kN/m)	Grip displacement at ultimate pullout load (mm)
195.6	6	201.2	9.48	30.0

4.1 Geogrid displacement measurements along the loading direction

The confined displacements of the geogrid specimen along the loading direction are plotted in Figure 4(a) for different frontal load levels. Figure 4(b) shows the relationship between the frontal unit tension and junction displacements in this test.

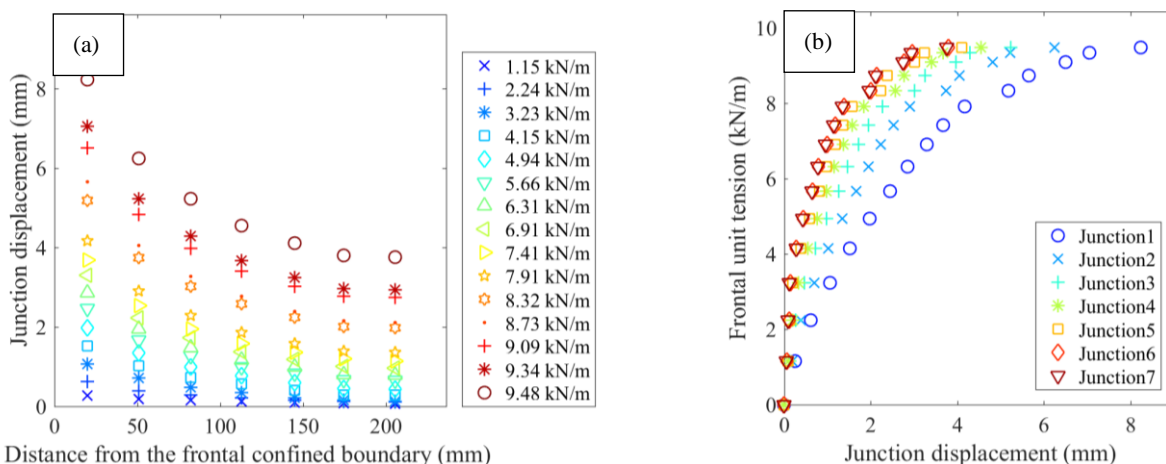


Figure 4. Geogrid displacement tracking in the prototype test: (a) geogrid displacement distribution along the loading direction; (b) the relationship between the frontal unit tension and junction displacements.

4.2 Soil displacement measurements along the loading direction

The laser was shot from the frontal view of the transparent soil model (see configuration in Figure 1), with the distance between the laser plane and the transparent side wall (the wall on the left-hand side in Figure 1) being 75 mm. As previously discussed, soil section in front of the geogrid (i.e. the section without rib shadows shown in Figure 2(a)) was selected as the correlation area to track the soil displacements along the loading direction. In this prototype test, several soil displacement profiles along both the loading (vertical) and the normal (horizontal) directions (shown in Figure 2(a)) in the correlation area of the laser illuminated plane were selected, as shown in Table 4.

Table 4. Locations of soil displacement profiles the loading (vertical) and the normal (horizontal) directions.

Profiles along the loading (vertical) direction, distance from the geogrid plane, h (mm)	Profiles along the normal (horizontal) direction, distance from the frontal confined boundary, v (mm)
≈ 0 (close to geogrid plane)	60
10	100
20	140
40	180

Figure 5 provides the distribution of soil displacements (along the loading direction) at planes located at four different distances from the geogrid for increasing levels of frontal load.

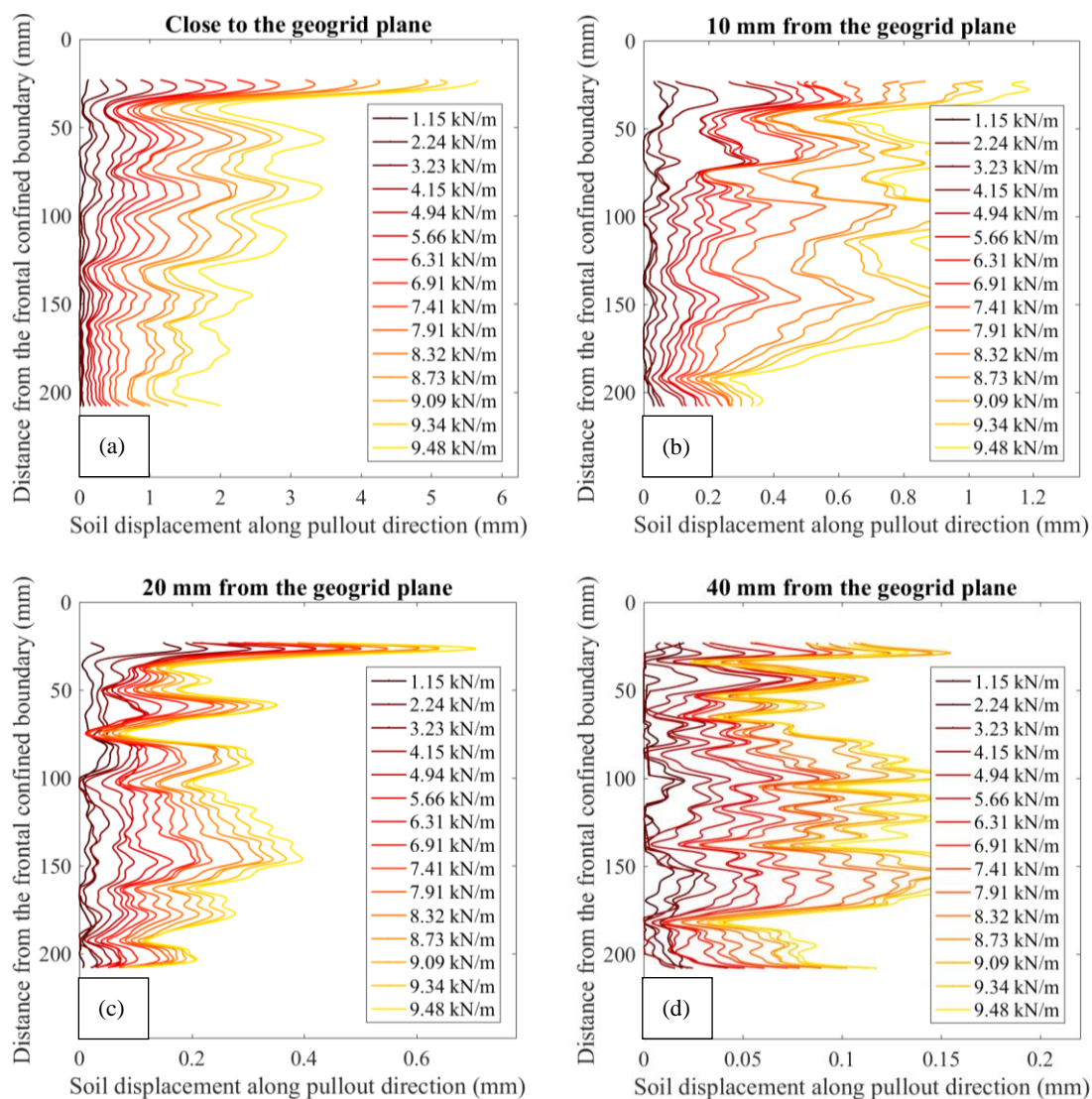


Figure 5. Soil displacement profiles along the loading direction in the laser-illuminated plane: profiles (a) close to, (b) at 10 mm from, (c) at 20 mm from, and (d) at 40 mm from the geogrid plane.

In the side-view images, 1 pixel represents 0.12 mm, therefore, the resolution of the DIC calculation is 0.012 mm (0.1 pixel). With such a high resolution, the results in Figure 5 demonstrates the general trends of soil displacement distribution for different frontal load levels. Overall, the displacement information in Figure 5(a) presents the best-quality results from the DIC calculation, compared to the results at larger distances from the geogrid plane. At the soil-geogrid interface (Figure 5(a)), the maximum and minimum soil displacements at the time of pullout failure were about 5.7 mm and 1.3 mm respectively. On the other hand, Figure 4 shows the maximum and minimum junction displacements at the stage of pullout failure were about 8.2 mm and 3.7 mm respectively. Consequently, the collected data also provides information suitable to define the relative displacements between soil and geogrid.

4.3 Profiles showing development of the soil shear band

The development of soil shear bands along the soil-geogrid interface could also be evaluated by tracking the soil displacements in the laser illuminated plane. Specifically, four different soil displacement profiles (Table 4) in the direction perpendicular to the geogrid, within the correlation area were selected for evaluation. The profiles are presented in Figure 6.

The results presented in Figure 6 defines comparatively smooth shapes of shear band profiles at the different distances from the frontal confined boundary. The results presented in Figure 5 and Figure 6 suggest that, if the distance from the geogrid plane is larger than 40 mm, the soil displacements were below 0.2 mm, which is about 0.05 times of the median size of the granular particles ($D_{50}=3.9$ mm). Also, in most cases, no significant displacements were obtained at distances exceeding 40 mm from the geogrid plane. Therefore, for the applied normal pressure (27.6 kN/m²), the depth of the influence zone defined by the interaction of the selected geogrid and the transparent soil used in this study can be considered to be approximately 40 mm.

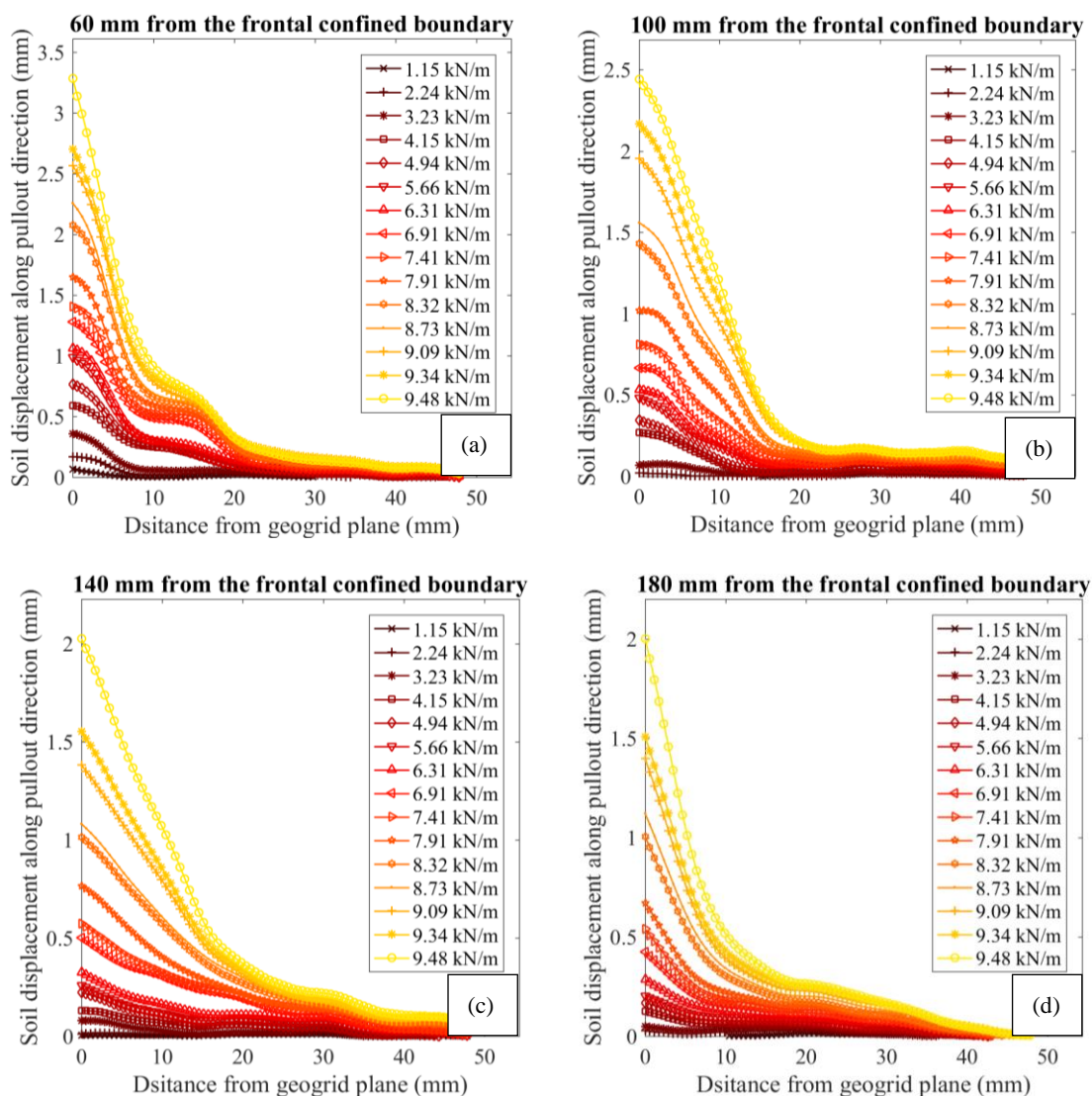


Figure 6. Soil displacement profiles along the normal direction in the laser-illuminated plane: profiles (a) at 60 mm, (b) 100 mm, (c) 140 mm, and (d) 180 mm from the frontal confined boundary.

5 SUMMARY AND CONCLUSION

A new experimental system was developed in this study, which involved the use of transparent soil with laser aided imaging. The system was found to be adequate to non-intrusively capture the deformations of both geogrid specimens and soil particles. Based on the test results, the following conclusions can be drawn:

- (1) Unlike the measurements from physical sensors in traditional pullout tests, the experimental setup developed in this study was found to be adequate to non-intrusively capture geogrid displacements without creating physical disturbances at the soil-geosynthetic interface.
- (2) The use of a collimated beam resulted in well-defined individual particles in the illuminated plane of the soil model. Consequently, soil displacements could also be non-intrusively measured during testing.
- (3) Digital image correlation (DIC) was found facilitate quantifying both the deformation of the confined geogrid specimen and the displacements of soil particles from the collected images.
- (4) The overall trends of the soil displacement profiles obtained in this study indicated that, for the normal pressure considered in this study (27.6 kN/m²), the depth of the influence zone within the soil next to the soil-geogrid interface was about 40 mm.

Overall, the developed experimental apparatus in conjunction with the displacement measurement technology used in this study, were found to represent a powerful tool to identify the impact of geogrid type on the load transfer mechanisms between soil and reinforcement.

ACKNOWLEDGEMENTS

The authors greatly appreciate the support provided by Tensar International Corporation. The authors also gratefully acknowledge Dr. Julio Ferreira who finished the initial design of the experimental setup used in this study.

REFERENCES

- ASTM D4439-15a, 2015. Standard Terminology for Geosynthetics. ASTM International, West Conshohocken, Pennsylvania. Retrieved from www.astm.org
- Chini, C.M., Wallace, J.F., Rutherford, C.J., Peschel, J.M., 2015. Shearing Failure Visualization via Particle Tracking in Soft Clay Using a Transparent Soil. *Geotech. Test. J.* 38, 20140210.
- Ezzein, F. M., & Bathurst, R. J, 2011. A Transparent Sand for Geotechnical Laboratory Modeling. *ASTM Geotech. Test. J.* 34, 590–601.
- Ferreira, J.A., Zornberg, J.G., 2015. A Transparent Pullout Testing Device for 3D Evaluation of Soil–Geogrid Interaction. *Geotech. Test. J.* 38, 686–707.
- Ferreira, J.A.Z., 2013. Evaluation of soil-geogrid interaction at different load levels using pullout tests and transparent soil (Ph.D. Dissertation). The University of Texas at Austin, Austin, Texas.
- Iskander, M., 2010. Modelling with transparent soils: Visualizing soil structure interaction and multi phase flow, non-intrusively. Springer Science & Business Media.
- Jones, E., 2015. Documentation for Matlab-based DIC code, Version 4. University of Illinois, Champaign County, Illinois.
- Koerner, R.M., 2012. *Designing with Geosynthetics - 6Th Edition*. Xlibris Corporation.
- Ochiai, H., Otani, J., Hayashic, S., Hirai, T., 1996. The pull-out resistance of geogrids in reinforced soil. *Geotext. Geomembr.* 14, 19–42.
- Peng, X., Zornberg, J.G., 2017. Evaluation of Load Transfer in Geogrids for Base Stabilization Using Transparent Soil. *Procedia Eng.* 189, 307–314.
- Roodi, G.H., and Zornberg, J.G., 2017. Stiffness of Soil-geosynthetic Composite under Small Displacements. II: Experimental Evaluation. *J. Geotech. Geoenviron. Eng. ASCE*, Vol. 143, No. 10, October.
- Teixeira, S.H., Bueno, B.S., Zornberg, J.G., 2007. Pullout resistance of individual longitudinal and transverse geogrid ribs. *J. Geotech. Geoenvironmental Eng.* 133, 37–50.
- Wallace, J. F. and Rutherford, C. J., 2015. Geotechnical Properties of Laponite Rd, *Geotech. Test. J.*, Vol. 38, No. 5, 2015, pp. 574-587
- Wilson-Fahmy, R.F., Koerner, R.M., 1993. Finite element modelling of soil-geogrid interaction with application to the behavior of geogrids in a pullout loading condition. *Geotext. Geomembr.* 12, 479–501.
- Ziegler, M., Timmers, V., 2004. A new approach to design geogrid reinforcement, in: *Proceedings of the 3rd European Geosynthetics Conference*.
- Zornberg, J.G., Roodi, G.H., and Gupta, R., 2017. Stiffness of Soil-geosynthetic Composite under Small Displacements. I: Model Development. *J. Geotech. Geoenviron. Eng. ASCE*, Vol. 143, No. 10, October.